Petroleum Science 23 (2026) 2885–2901

Contents lists available at ScienceDirect

Petroleum Science

journal homepage: www.keaipublishing.com/en/journals/petroleum-science

Original Paper

Wax deposition characteristics under oil-water two-phase stratified flow in pipeline

Hui-Shu Liu [a,b], Ji-Miao Duan [b,*], Yong-Xiang Huang [b], Hao-Nan Li [b], Hui-Rong Huang [a,**], Shi-Ming Chen [b], Jun-Zhe Jiang [b]

[a] School of Petroleum Engineering, Chongqing University of Science and Technology, Chongqing, 401331, China
[b] PLA Joint Logistics Support Force University of Engineering, Chongqing, 401331, China

ARTICLE INFO

Article history:
Received 8 September 2025
Received in revised form
16 November 2025
Accepted 13 January 2026
Available online 20 January 2026

Edited by Teng Zhu and Meng-Jiao Zhou

Keywords:
Wax deposition
Oil-water two-phase flow
Stratified flow
Heat and mass transfer

ABSTRACT

Wax deposition in subsea pipelines transporting waxy crude oil under oil-water stratified flow remains a critical flow assurance challenge. This study systematically investigates wax deposition characteristics using an experimental flow loop that simulates deep-sea conditions. Experiments were conducted with waxy simulated oil and deionized water under varying superficial velocities of both phases. Results show a crescent-shaped deposition layer exclusively on the upper oil-wetted wall, with no deposition on the water-contacted lower wall. Notably, the deposit near the oil-water interface exhibits higher wax content and enriched heavy components compared to the top wall, indicating localized aging behavior. A key finding is that increasing oil or water superficial velocity reduces deposition thickness but enhances wax content and promotes aging. The deposit mass per unit area correlates negatively with oil-phase actual velocity, while wax content and heavy component concentration show strong positive correlations. This work provides novel insights into the circumferential heterogeneity and phase-specific aging of wax deposition in stratified oil-water flow, offering a foundation for improved predictive models.

1. Introduction

Under low-temperature conditions in deep water and intense heat exchange, the temperature of crude oil near the pipe wall in subsea waxy oil pipelines decreases below the wax appearance temperature (WAT). Consequently, dissolved wax molecules near the pipe wall crystallize into solid-phase structures, forming three-dimensional networks that deposit via free surface energy onto the pipe wall or existing deposit layers (Wang et al., 2022, 2024). This deposition reduces the pipeline's effective flow area, diminishes transportation capacity, increases energy consumption, and may lead to pipeline blockages—posing significant threats to subsea production safety and flow assurance (Yao et al., 2023; Akbari et al., 2024). As documented in Fig. 1, wax deposition issues have been reported across major global oil-producing regions (Zheng, 2017), establishing this phenomenon as a universal challenge for waxy oil pipelines.

With the proliferation of deepwater and ultra-deepwater drilling in oil and gas production, water is invariably present in waxy oil transmission pipelines (Shafiei et al., 2023; Lekomtsev et al., 2018). Furthermore, during late-stage field extraction, reservoir pressure decline typically necessitates water injection techniques, making oil-water two-phase flow ubiquitous in crude oil transportation. Stratified flow, a prevalent flow pattern in oil-water systems, serves as the fundamental basis for studying complex flow regimes. Therefore, investigation into wax deposition characteristics and predictive modeling for waxy oil-water stratified flow under deepwater low-temperature conditions holds critical importance for both deepwater resource development and pipeline operational safety.

Stratified flow represents a common pattern in oil-water two-phase pipe flow and serves as a fundamental basis for investigating other flow regimes. Nevertheless, experimental research on wax deposition within oil-water stratified flow remains limited due to experimental complexities and the multifaceted nature of

* Corresponding author.
** Corresponding author.
E-mail addresses: duanjimiao@126.com (J.-M. Duan), hryh@cqust.edu.cn (H.-R. Huang).

Peer review under the responsibility of China University of Petroleum (Beijing).

https://doi.org/10.1016/j.petsci.2026.01.016

Fig. 1. Overview of wax deposition problems reported around the world (red dots mark: fields where wax deposition occurs) (Zheng, 2017).

influencing factors. Consequently, only a small number of scholars have undertaken experimental studies focused on wax deposition characteristics, and even fewer have developed effective predictive models. Bordalo and Oliveira (2007) employed simulated oil to examine wax deposition in stratified and annular flows. The findings indicate deposition in stratified flow is confined to the upper section of the pipe wall. In contrast, annular flow exhibits deposition across the pipe wall, despite separation of the oil phase from the wall by a water ring. Although this water film inhibits contact between wax particles and the pipe surface, its effectiveness is constrained by the thickness, discontinuous, and intermittent nature of the film. Anosike (2007) separately investigated deposition characteristics using an oil-water two-phase annular channel apparatus, encompassing stratified flow, oil-in-water dispersed flow, water-in-oil dispersed flow, and double-dispersed flow. Observations revealed significant variations in both wax deposition distribution along the inner pipe wall and oil-water heat transfer characteristics across different flow patterns, thereby influencing deposition behavior. Specifically under stratified flow conditions, deposition occurs exclusively on pipe wall regions in direct contact with the oil phase. The deposit layer demonstrates uniform circumferential distribution (except near oil-water interface regions) and exhibits a relatively compliant texture, comparable to deposits formed under single-phase laminar flow. Additionally, the deposition layer is water-free, with the thickness decreasing and wax content increasing with elevated water phase superficial velocity.

Hoffmann et al. (2012) investigated wax deposition in oil-water stratified flow using a 2-inch annular channel apparatus with North Sea condensate and formation water. Experiments were conducted at oil-water mixture flow rates of 5 m^3/s and 10 m^3/s, where deposition layer thickness distributions along the pipe circumference were quantified via laser measurement techniques. As illustrated in Fig. 2, no deposition occurred on the lower pipe wall contacting the water phase, while wax accumulation was confined to the upper oil-contacting region with non-uniform thickness distribution. Gas chromatographic analysis of deposit carbon number distributions revealed that deposition layer formation involved both molecular diffusion and gelation mechanisms. Critically, reduced mixture flow rate (from 10 m^3/s to 5 m^3/s) corresponded to decreased oil phase shear stress, enhanced gelation, increased deposit thickness, and lower long-chain alkane content in deposits, resulting in carbon number distributions closer to the bulk oil phase. Additionally, at a fixed flow rate of 5 m^3/s, higher water content reduced deposit thickness, shifted deposit alkane distributions toward oil-phase characteristics, and amplified gelation effects. Separately, Quan et al. (2015) examined deposition in a system featuring oil-in-water emulsion stratified above free water. Circumferential deposit distribution measurements were achieved using a custom-designed laser thickness gauge. Their data indicate that increased oil-water mixture flow rate expanded the emulsion phase fraction within the pipe cross-section. This means that the deposition thickness at the pipe vertex increases as the gelation within the deposition layer intensifies.

Piroozian et al. (2017) investigated the flow patterns of waxy oil-water two-phase pipe flow and identified nine distinct flow patterns. They conducted a theoretical analysis to elucidate the formation mechanisms of each pattern and categorized six specific flow patterns based on the distribution characteristics of wax deposition on the pipe wall, as illustrated in Fig. 3. In these experimental flow patterns, wax deposition primarily formed crescent-shaped accumulations at the pipe top. Critically, deposition occurred only at higher oil-water mixture flow rates, with deposit thickness increasing proportionally to elevated flow rates of both water and oil phases. This positive correlation between flow rate and deposit thickness directly contradicts the inverse relationship reported by Hoffmann et al. (2012) for wax deposition.

Current understanding of wax deposition characteristics remains fragmented, preventing consensus on formation mechanisms. This knowledge gap is more pronounced for predictive modeling of wax deposition. Huang et al. (2011a, 2011b, 2011c) developed a parallel-plate oil-water stratified flow deposition model based on molecular diffusion, integrated with computational simulations of flow, heat, and mass transfer. Their analysis demonstrated that neglecting axial variation in oil-water interface position during non-isothermal flow leads to significant underestimation of deposition rates. Critically, the aqueous phase alters heat and mass transfer characteristics, reducing deposition rates relative to single-phase systems, a finding which contradicts the experimental observations of Hoffmann et al. (2012). Hoffmann et al. (2012) attributed reduced deposition to: (i) decreased available deposition surface area from partial wall-water contact (mass transfer perspective), and (ii) reduced oil cooling rates from aqueous-phase energy contribution and added radial thermal resistance (heat transfer perspective). However, the model is inapplicable to circular pipes due to fundamental differences in heat transfer dynamics and increased geometric complexity. Quan et al. (2015) established a wax deposition model for oil-in-water emulsion-water laminar pipe flow based on molecular diffusion and gelling mechanisms. By comparing the calculation results of only considering the molecular diffusion effect it was found that the calculation results of the model without considering the gelling effect had a large difference with the experimental values. However, the model does not elucidate the reasons behind the relatively uniform distribution of the deposition layer in the annulus above the pipeline cross-section, nor does it provide insights into how the thickness of this deposition layer varies with factors such as water content and apparent liquid phase flow rate.

Among the existing oil-water two-phase wax deposition models, one-dimensional models occupy a dominant position, while the specific flow, heat and mass transfer processes specific to stratified flow deposition have not been systematically analyzed. Only generalized descriptions of deposit distribution patterns in pipe cross-sections have been provided, without quantitative descriptions of the effects of oil-phase and water phase superficial velocities. To establish and validate a computational model for wax deposition in oil-water stratified flow, experiments were conducted using an annular flow apparatus with waxy simulated oil and deionized water. Testing was performed at varying superficial velocities of both aqueous and oil phases. The cross-sectional distribution characteristics of wax deposition were investigated,

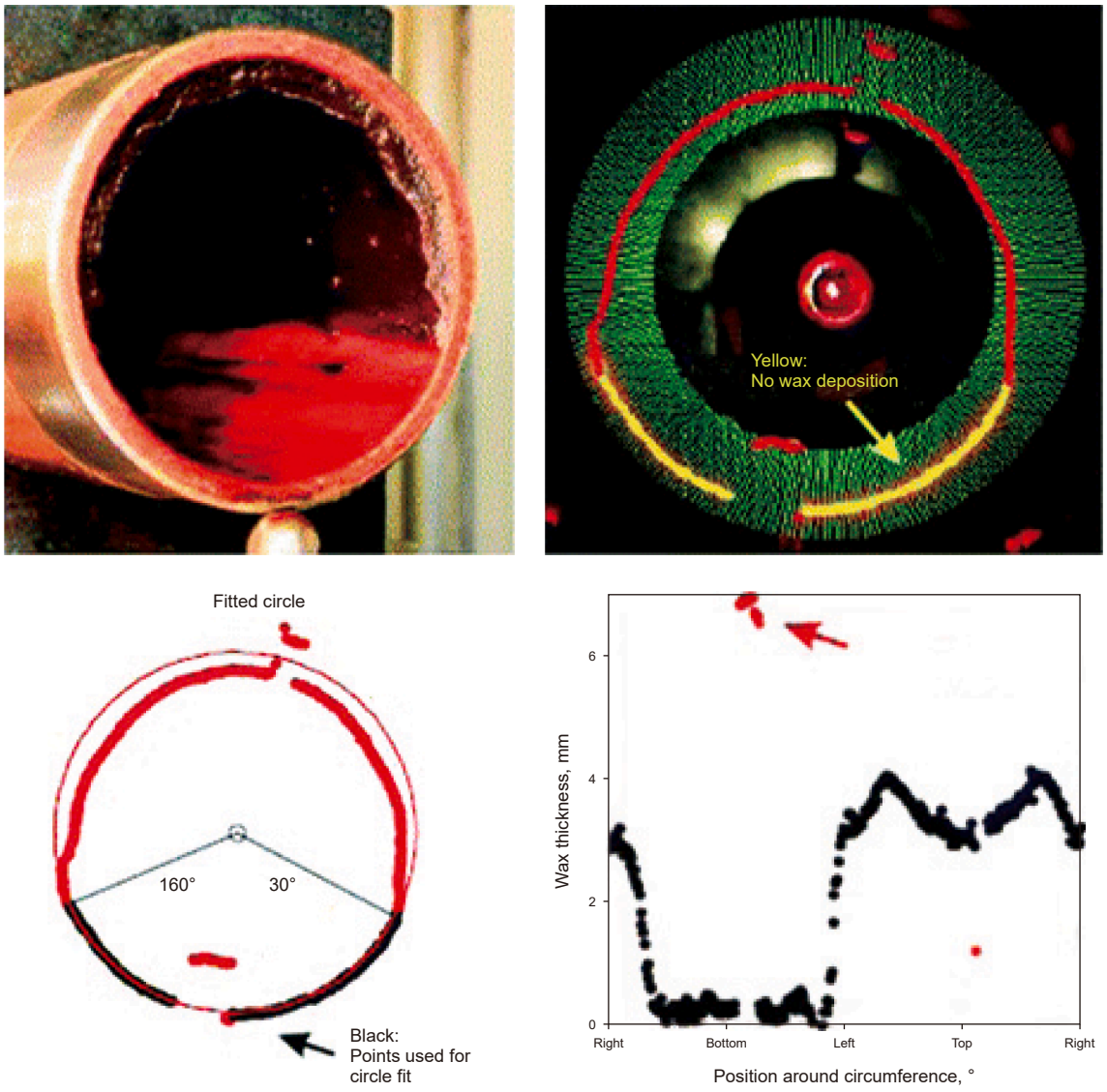

Fig. 2. Distribution of wax deposition in the oil-water two-phase stratified flow (Hoffmann et al., 2012).

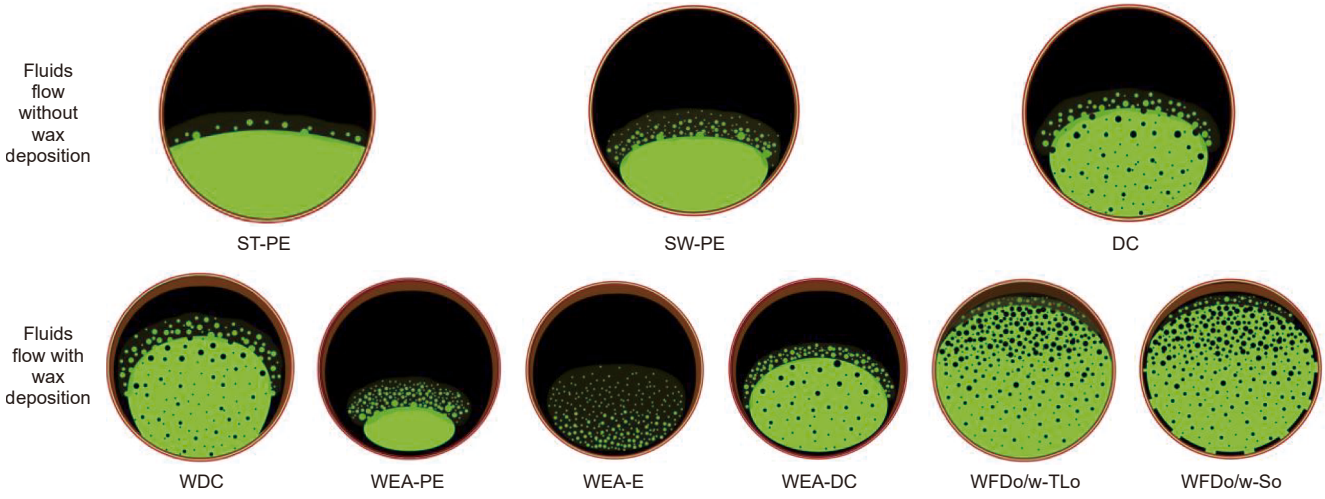

Fig. 3. Flow pattern map of waxy crude oil-water two-phase stratified flow in horizontal pipes (Piroozian et al., 2017).

along with the influence of aqueous and oil phase superficial velocities on deposition. Wax content and carbon number distributions of deposits were analyzed by high-temperature gas chromatography (HTGC) at distinct circumferential positions within the pipe cross-section.

2. Experimental

Due to the long duration of the oil-water laminar wax deposition loop test, the oil and water phases are subjected to continuous shearing by the pump during the test, which makes it very easy to form emulsion. In order to ensure stable oil-water laminar flow in the ring channel, the oil and water phases enter the deposition test section of the ring channel separately, and an oil-water separator with heating function is set up at the exit of the ring channel to keep the oil and water phases warm, and the oil and water are separated sufficiently and then re-enter the ring channel again through independent pipelines and pumps.

2.1. Physical properties of fluid media

The oil-water stratified flow wax deposition experiments employed a concentric annular apparatus to achieve stable flow patterns. Waxy simulated oil and deionized water served as experimental media to enhance phase separation efficiency. The simulated oil comprised 7 wt% fully refined paraffin wax (C_{24}–C_{42} carbon distribution) from Daqing Petrochemical and ExxonMobil Exxsol D80 solvent oil (de-aromatized, desulfurized; C_{12}–C_{15} carbon distribution; colorless non-volatile liquid; properties in Table 1). Deionized water exhibited resistivity >15 MΩ cm.

The solidification point of the waxy simulated oil (tested by GB/T 510-2018: Method for Determination of solidification point for petroleum products; approximately equivalent to ASTM D97 pour point + 3 °C for waxy oils) was measured as 23 °C. The interfacial tension between oil and water was tested using the spin-drop tensiometer (TX-500, Kono Industries Co., Ltd, USA), and the interfacial tension measured at 25 °C was 38.5 mN/m. The viscosity-temperature characteristics of the waxy simulated oil were characterized by the rotational rheometer (MCR 302, Anton Paar GmbH, Austria). The viscosity-temperature characteristics of the waxy simulated oil under different shear rates are shown in Fig. 4.

The thermal analysis curve of the waxy simulated oil were measured by the differential scanning calorimeter (DSC 200 F3, NETZSCH-Gerätebau GmbH, Germany), as shown in Fig. 5. It can be seen from the thermal analysis curve that as the temperature decreases, the heat flux density signal when wax crystals precipitate in the oil sample increases sharply. At this time, the corresponding temperature is the wax crystal precipitation point, which is 25.1 °C for the waxy simulated oil.

Based on the thermal analysis curve and latent heat of crystallization calculations, the variation rule of wax precipitation in the waxy simulated oil with temperature is shown in Fig. 6. Wax crystallization initiates at the precipitation point (25 °C), with precipitated wax mass progressively increasing as temperature decreases to −20 °C, where crystallization completes. Given that operational temperatures in field crude oil pipelines and deposition experiments substantially exceed −20 °C, and considering the

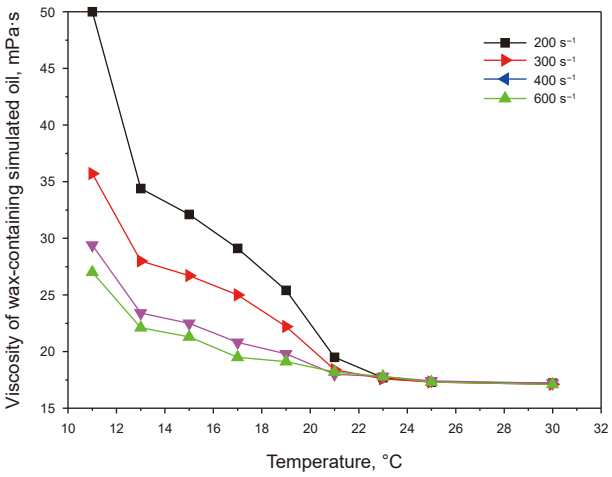

Fig. 4. Viscosity-temperature characteristic curve of the waxy simulated oil.

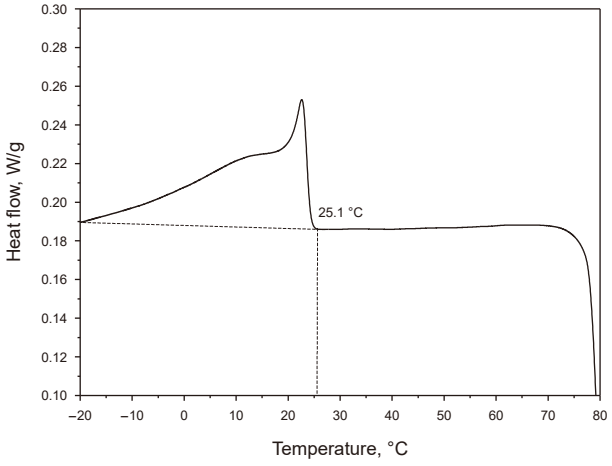

Fig. 5. DSC thermal analysis curve of the waxy simulated oil.

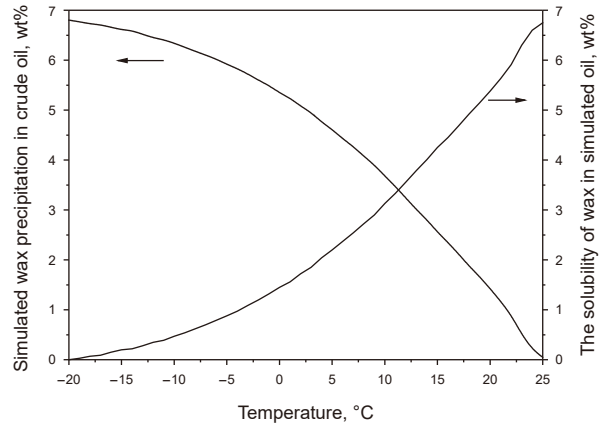

Fig. 6. Wax precipitation characteristics and wax solubility curve of the waxy simulated oil.

Table 1
Physical properties of D80 solvent oil.

Petroleum product	Density, kg/m^3	Kinematic viscosity, mm^2/s	Flash point, °C	Initial boiling point, °C
D80	795.0 (15.0 °C)	2.09 (25.0 °C)	80.0	204

dominant role of wax concentration gradients in deposition dynamics, the complete precipitation state at −20 °C serves as a valid reference for characterizing deposition behavior.

The carbon number distribution of the waxy simulated oil was analyzed by high-temperature gas chromatography (GC 8890, Agilent Technologies, USA), with results shown in Fig. 7. The carbon number distribution analysis reveals the wax component of the waxy simulated oil spans C12–C42 with broad dispersion. D80 solvent oil exhibits a narrow C12–C15 distribution, while paraffin wax displays a wider C24–C42 range. The carbon number distributions of D80 solvent oil and paraffin wax show complete separation with no overlapping carbon numbers. This distinct separation enables unambiguous differentiation between wax and oil components in the waxy simulated oil, supporting precise analysis of deposited wax carbon number distributions.

2.2. Experimental methods and procedures

Fig. 8 shows the schematic diagram of the wax deposition experimental setup for oil-water two-phase stratified flow. The oil-water two-phase stratified flow wax deposition experimental loop is mainly composed of oil supply system, water supply system, gas supply system, piping system, separation system, temperature control system and data measurement and signal acquisition 7 parts. The functions and related details of each part can be obtained from the supplementary information. The 30 m oil-water pipeline system utilizes 304 stainless steel tubing with 25.4 mm internal diameter. A water jacket connected to a bath controller maintains temperature throughout the loop, enabling wax deposition experiments under single-phase oil or oil-water two-phase flow conditions. Oil and water phases from the respective tanks are delivered through dedicated transfer pumps and pipelines to a Y-shaped mixer, entering the main annular flow section. With the progress of the experiment, the waxy simulated oil enters the wax deposition test section. Here, when the temperature of the fluid medium comes into contact with the pipe wall at a lower temperature, wax begins to deposit on the pipe wall. Subsequently, the fluid medium enters the oil-water separator for phase separation and then returns to the storage tank to complete the cycle. The detailed wax deposition loop devices are provided in Supplementary Material.

The oil-water two-phase stratified flow wax deposition loop experiment mainly includes the preparation of waxy simulated oil, the selection of stable flow conditions for oil-water two-phase stratified flow, wax deposition occurrence and growth, wax deposition measurement, and wax dissolution. The main steps are as follows:

(1) To ensure experimental repeatability and result stability, solvent oil was added to the oil tank and heated to 60 °C prior to each experimental run. Paraffin wax was subsequently weighed and added to achieve a 7% mass fraction concentration.
(2) The waxy simulated oil underwent thermal pretreatment at 60 °C for 6 h to ensure complete wax crystal dissolution. Following pretreatment, the circulating water tank temperature was adjusted to cool the simulated oil to the required experimental temperature while simultaneously regulating the hot water tank temperature.
(3) Predetermined volumes of simulated oil and water were transferred to the oil-water separator. The separator heating device and temperature controller were activated concurrently.
(4) The circulating coolant temperature of the thermostatic water bath for the test section and the temperatures of all other thermostatic water baths in the piping system were adjusted to the temperatures required for the experiment.
(5) When the temperature of the fluid medium in the oil tank, water tank, and separator reached the experimental temperature and remained stable, the oil transfer pump and water transfer pump were turned on. The rotational speed was adjusted so that the flow rate of the oil phase and water phase reached the experimental set value. Simultaneously, the data acquisition system was started.
(6) After reaching the preset deposition duration, the oil transfer pump, water transfer pump, and relevant valves were deactivated. Air blowing was then commenced to evacuate residual oil and water from the pipeline to the separator.
(7) After the blowing was completed, the wax deposition test section was disassembled. The distribution characteristics of the deposition layer were observed, the weight of the deposit was measured, the deposit was sampled, and the carbon number distribution of the deposit was analyzed by high-temperature gas chromatography.

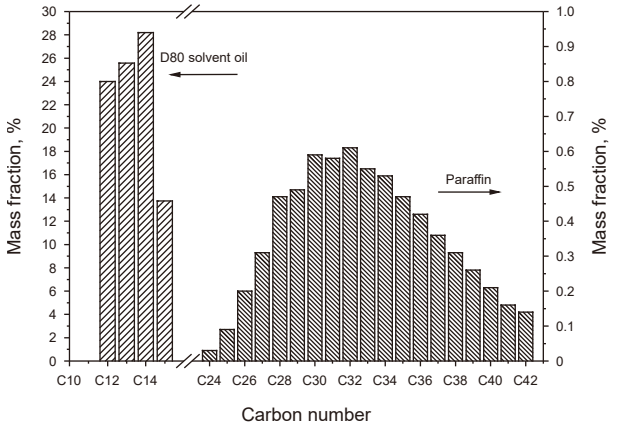

Fig. 7. Carbon number distribution of the waxy simulated oil.

2.3. Experimental condition setting

The experiments were conducted by adjusting the temperature controllers of the oil tank, water tank, and wax deposition test section to maintain the temperature of the oil and water phase media at 30 °C and the temperature of the cooling medium at 15 °C. The temperatures of the oil and water phases were controlled using frequency converters. The flow rates of different oil and water phases were controlled by adjusting the pump speed through a frequency converter. According to the transparent Plexiglas observation section set up in the experimental loop system, the superficial velocities of the oil phase were selected to be 0.09, 0.15 and 0.30 m/s for the oil-water two-phase stratified flow, and the apparent flow rates of the water phase were selected to be 0.05, 0.11, and 0.34 m/s, and the inlet water content ranged from 15% to 80%. For wax deposition durations of 4, 12, and 24 h, the mass of deposited wax was measured by weighing. Deposit composition analysis via HTGC was performed at each time point to determine the wax content in the deposits. Components above C24, as measured by HTGC, were selected for analysis to facilitate the presentation of experimental results and conclusions. To investigate the effect of oil-water two-phase stratified flow heat transfer on wax deposition, single-phase oil flow wax deposition

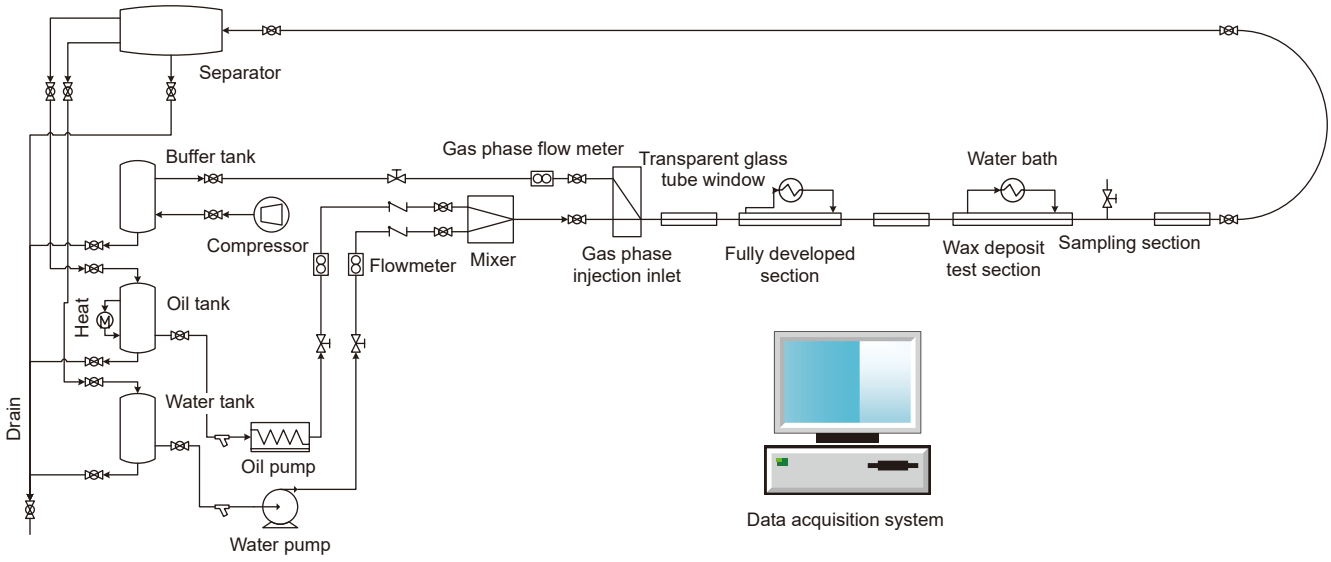

Fig. 8. Schematic diagram of wax deposition experiment setup for oil-water two-phase stratified flow.

experiments were conducted at oil phase superficial velocities of 0.10, 0.20, and 0.40 m/s, which encompassed the actual oil-phase flow rate range observed during the two-phase experiments. The comprehensive wax deposition loop experimental program, detailed in Table 2, comprised a total of 36 experimental runs.

2.4. Scope and limitations of the experimental study

It is crucial to delineate the scope and inherent limitations of this experimental study to clarify the applicability of the presented findings. The conclusions drawn herein are primarily valid under the following specific conditions:

(1) Flow pattern: The investigation was exclusively conducted under stable, laminar oil-water stratified flow. The deposition characteristics may differ significantly in other flow regimes, such as dispersed or slug flow, which are common in field operations.
(2) Fluid properties: The working fluids consisted of a model waxy oil (a binary mixture of paraffin wax and solvent oil) and deionized water. The absence of natural surfactants, asphaltenes, and resins present in live crude oils means that the effects of emulsification and the complex interactions between different crude fractions on wax deposition were not captured.
(3) Operational parameters: The experiments were performed within a defined range of superficial velocities (oil: 0.09–0.30 m/s; water: 0.05–0.34 m/s) and at a fixed temperature differential (oil/water at 30 °C, coolant at 15 °C). Extrapolation of the results beyond these ranges should be done with caution.
(4) Geometric scale: The study utilized a laboratory-scale flow loop with a 25.4 mm internal diameter. Scale effects, which could influence flow hydrodynamics and heat transfer in large-diameter pipelines, were not investigated.

3. Results and discussion

3.1. Repeatability of experimental results

The repeatability of experiment is important for ensuring the credibility and reliability of the experimental results. According to the requirements, it is necessary to do a full set of duplication flow loop experiment. Due to the complexity and long duration of the wax deposition experiment, three sets (the second, eighth and tenth) were selected for the repeatability, as shown in Table 2. The three sets of experiments were conducted thrice, for wax deposition durations of 24 h. The average, standard deviation, coefficient of variation of the wax deposition mass and the wax content

Table 2
Experimental conditions for wax deposition in an oil-water two-phase stratified flow loop.

Group	Water phase volumetric flow rate, m^3/h	Oil phase volumetric flow rate, m^3/h	Water phase superficial velocities, m/s	Oil phase superficial velocities, m/s
1	–	0.11	–	0.10
2	–	0.23	–	0.20
3	–	0.45	–	0.40
4	0.06	0.10	0.05	0.09
5	0.06	0.17	0.05	0.15
6	0.06	0.34	0.05	0.30
7	0.12	0.10	0.11	0.09
8	0.12	0.17	0.11	0.15
9	0.12	0.34	0.11	0.30
10	0.38	0.10	0.34	0.09
11	0.38	0.17	0.34	0.15
12	0.38	0.34	0.34	0.30

Table 3
The wax deposition mass for the three repeated experiments.

Group	First, g	Second, g	Thirth, g	Average, g	Standard deviation, g	Coefficient of variation, %
2	127.65	125.03	126.35	126.34	1.31	1.04
8	45.65	43.36	46.53	45.18	1.64	3.62
10	29.69	27.63	28.45	28.59	1.04	3.63

Table 4
The wax content in the deposision layer for the three repeated experiments.

Group	First, wt%	Second, wt%	Thirth, wt%	Average, wt%	Standard deviation, wt%	Coefficient of variation, %
2	21.60	20.75	21.23	21.19	0.43	2.01
8	22.98	21.95	23.54	22.82	0.81	3.53
10	23.37	21.85	22.50	22.57	0.76	3.39

in the deposision layer measured from the three repeated experiments are shown in Tables 3 and 4 respectively.

The standard deviations coefficient of variations of the wax deposition mass for the Group 2, 8, 10 three sets of experiments are both relatively small, indicating that the experiment has high repeatability and the experimental setup and methods are highly reliable. The results of the wax content in the deposition layer also indicate this point.

3.2. Analysis of wax deposition characteristics of single-phase pipe flow

The wax deposition mass and wax deposition mass per unit area under different oil phase superficial velocities are presented in Figs. 9 and 10, respectively. Both parameters exhibit an increase with both deposition time and oil phase superficial velocity. Furthermore, the disparity in wax deposition mass between different oil phase superficial velocities increases over time.

Fig. 11 presents the variation law of wax content in wax deposition with time under different oil phase superficial velocities. When the oil phase superficial velocity remains constant, the wax content in the deposits increases with time. This temporal increase indicates an “aging” phenomenon occurring within the deposition layer, suggesting a corresponding increase in deposit hardness over time. Concurrently, a higher oil phase superficial velocity corresponds to a higher wax content within the deposits. However, the rate of increase in wax content gradually diminishes as the oil phase superficial velocity increases, eventually tending towards stabilization.

Fig. 12 presents the variation in the carbon number distribution within the deposits under different deposition time conditions for an oil phase superficial velocity of 0.40 m/s. As deposition time increases, the proportion of high-carbon-number components

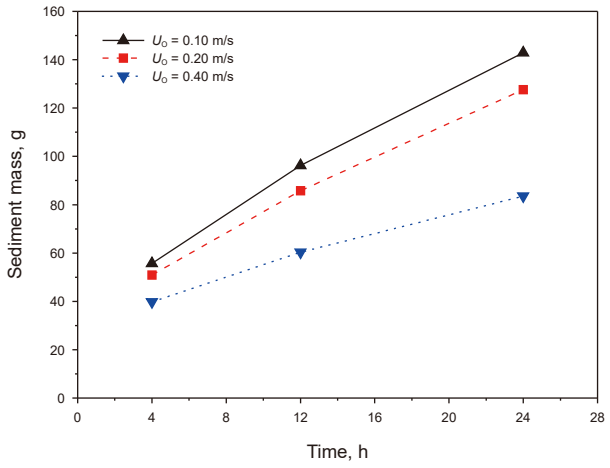

Fig. 9. Diagram of the variation law of wax deposition mass with time under different oil phase superficial velocities.

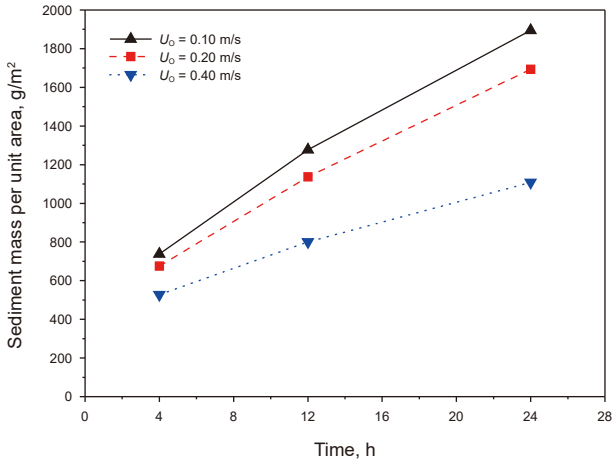

Fig. 10. Diagram of the variation law of wax deposition mass per unit area with time under different oil phase superficial velocities.

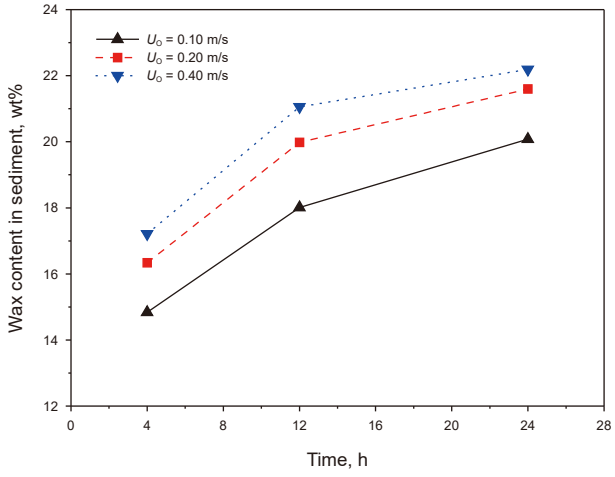

Fig. 11. Diagram of the variation law of wax content in deposition with time under different oil phase superficial velocities.

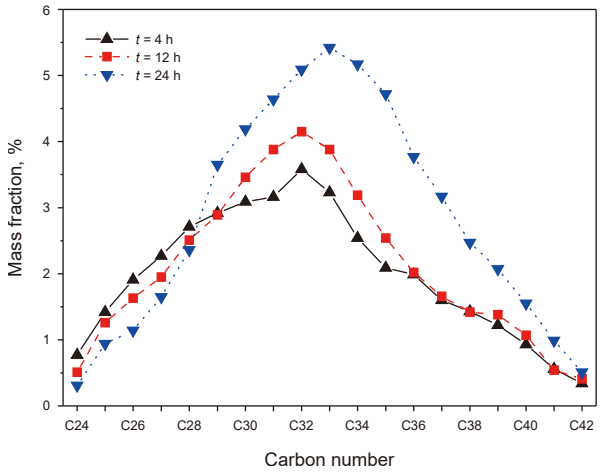

Fig. 12. Carbon number distribution in deposition under different deposition time conditions (U_o = 0.40 m/s).

(C29–C42) within the deposits increases, while the proportion of low-carbon-number components (C24–C28) decreases, corresponding to an increase in deposit hardness. According to the "aging" mechanism of wax deposition, with prolonged deposition time, wax molecules above C29 originating from the bulk oil flow, the deposit surface, or the shallow deposit layers utilize the liquid oil entrained within the wax deposition layer as a medium. These molecules continue to diffuse into the interior of the deposit layer, subsequently crystallizing and precipitating, thereby increasing the wax content within the deposit layer. Concurrently, as the concentration of wax molecules below C28 within the deposit layer exceeds that in the bulk oil flow, driven by this concentration gradient, molecules below C28 within the deposit layer counter-diffuse towards the oil flow. C28 represents the critical carbon number for this experimental condition.

Fig. 13 illustrates the effects of different oil phase superficial velocities on the carbon number distribution of deposits after 24 h of deposition. The results indicate that within the oil phase superficial velocity range of 0.10–0.40 m/s, increasing the oil flow rate exerts a pronounced effect on deposit composition. The enhanced shear stress associated with higher oil flow rates reduces the amount of oil entrained within the pipe wall deposits,

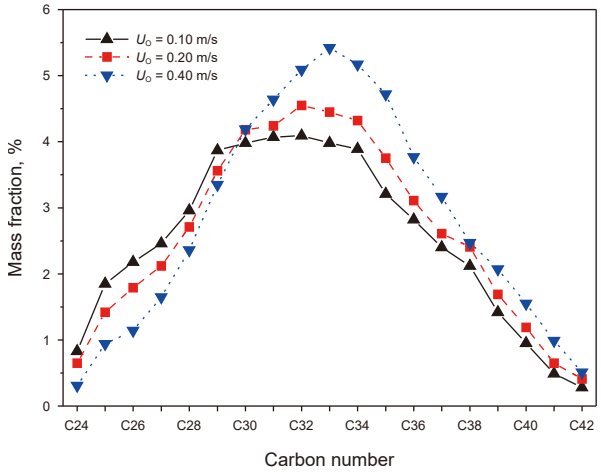

Fig. 13. Carbon number distribution in deposition under different oil phase superficial velocities.

thereby aggravating the "aging" effect within the deposit layer. This results in a decrease in low-carbon-number components and a significant increase in the proportion of high-carbon-number components. This phenomenon is primarily attributed to the higher oil phase superficial velocity intensifying convective heat transfer within the pipe. This enhanced heat transfer increases the temperature gradient at the deposit-oil flow interface, promoting the deposition of higher-molecular-weight fractions (high-carbon-number components).

The observed increase in wax content and the enrichment of high-carbon-number components with time and flow rate point to the occurrence of deposit aging. This phenomenon is attributed to a synergistic interplay between molecular diffusion and shear stress. The aging process is fundamentally driven by molecular diffusion, wherein dissolved wax molecules (particularly higher alkanes) from the bulk flow continue to diffuse into the deposit layer and precipitate, while entrapped liquid oil (richer in lighter components) diffuses out, driven by concentration gradients (Li et al., 2020; Huang et al., 2011). Shear stress, intensified at higher flow rates, acts as a critical accelerator of this process. It compacts the deposit matrix, reducing its porosity and the amount of occluded oil. This compaction shortens the internal diffusion path lengths and promotes a more effective expulsion of light components, thereby leading to a denser, harder deposit with an accelerated enrichment of heavy waxes. Therefore, while diffusion dictates the compositional shift, shear stress controls the kinetics and the final physical state of the aged deposit.

3.3. Analysis of wax deposition characteristics of two-phase pipe flow

3.3.1. Wax deposition characteristics of pipe cross sections

The circumferential distribution pattern of wax deposition on the pipe wall cross-section in oil-water two-phase stratified flow is closely related to the flow pattern, analogous to wax deposition behavior observed in oil-gas two-phase stratified flow (Goncalves and Matar, 2022; Chi et al., 2019; Duan et al., 2017). Different flow patterns yield distinct deposit distribution patterns and circumferential variations in deposit wax content (Anosike, 2007; Hoffmann et al., 2012; Piroozian et al., 2017). Therefore, to elucidate the wax deposition characteristics of oil-water stratified flow, investigation of local deposition characteristics across the pipe cross-section is essential.

3.3.1.1. Distribution of deposited layers on the pipe cross-section. Fig. 14(a) shows the morphology of the deposit layer on the inner pipe wall cross-section after disassembly, following 24 h of deposition under superficial oil-phase velocity U_{so} = 0.09 m/s and superficial water-phase velocity U_{sw} = 0.11 m/s. Under the oil-water laminar flow conditions, the deposit morphology exhibits a crescent shape. Wax deposition occurs only on the upper pipe wall section in contact with the oil phase. No wax deposition occurred on the lower pipe wall in contact with water. The main reason might be that the aqueous phase acted as a barrier, resulting in the pipe wall lacking direct contact with the oil phase. The thickness of the deposit layer on the entire cross-section of the pipe was measured at 20° intervals around the pipe using a square and a calibrated needle. The needle with scale has an accuracy of 0.05 mm. Considering that the needle may undergo slight deformation when inserted into soft deposits, it is estimated that the measurement error is within ±0.02 mm. The variation of deposit layer thickness with the angle (α) from the pipe center is shown in Fig. 14(b). The deposit layer near the top of the pipe wall ($\alpha \approx 0°$) has a relatively uniform thickness of approximately 4.71 mm.

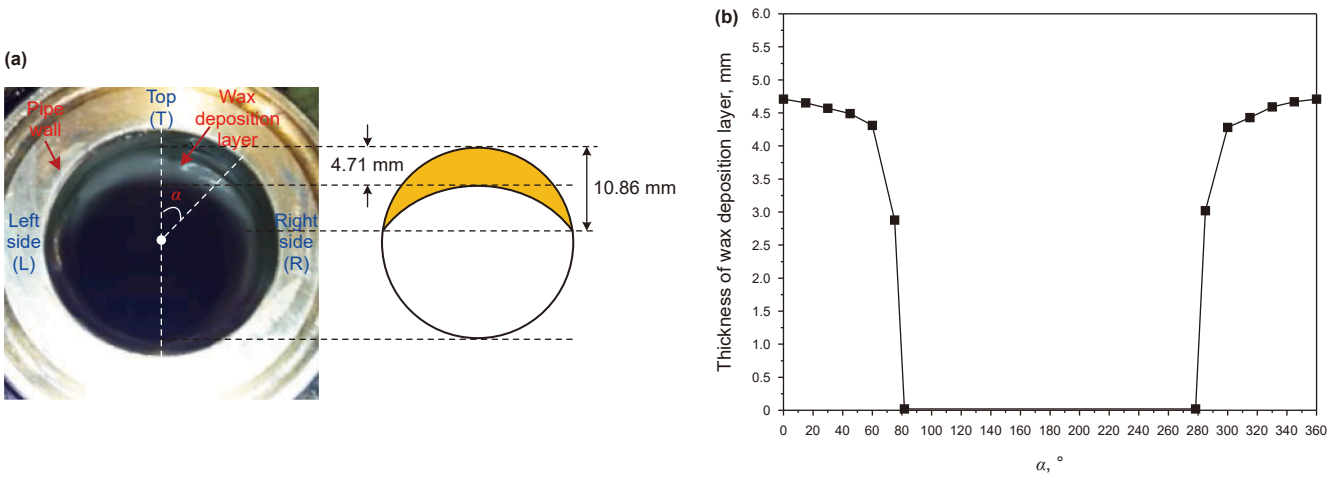

Fig. 14. Wax deposition layer morphology distribution on pipe cross-section: **(a)** Cross-sectional morphology distribution of deposition layer and **(b)** radial thickness distribution of deposition layer on pipe wall.

Progressing circumferentially along the pipe wall towards the oil-water interface, the deposit layer thickness decreases.

To further analyze wax deposition characteristics across the pipe cross-section, the deposition layer was divided into three parts: top (T), left side (L) and right side (R) of the contact part of the phase interface according to the distribution morphology of the deposition layer on the pipe wall. The wax contents of deposits from the top, left, and right pipe wall regions, measured via high-temperature gas chromatography, were 18.21%, 23.19%, and 22.96%, respectively. The wax contents of the left and right deposit layers were essentially identical. Relative to the top deposit layer, regions near the oil-water phase interface exhibited thinner deposits with higher wax content. This finding aligns with direct morphological observations: the deposit on the top inner pipe wall was softer, while deposits on the left and right sides were harder and firmer.

Fig. 15 exhibits the carbon number distributions of deposits from the top, left, and right pipe wall regions. The alkane compositions of the left and right deposits were similar, while the top deposit contained fewer high-carbon-number components. This result is consistent with the measured wax content data. Unlike single-phase flow, where the deposit-oil flow interface temperature and thermal boundary layer are uniformly distributed circumferentially, the oil-water two-phase stratified flow exhibits circumferential variation in this distribution. Different n-alkane components possess distinct physical properties (e.g., solubility, molecular diffusivity), leading to differing mass transfer and precipitation characteristics at the deposit surface (Li et al., 2020).

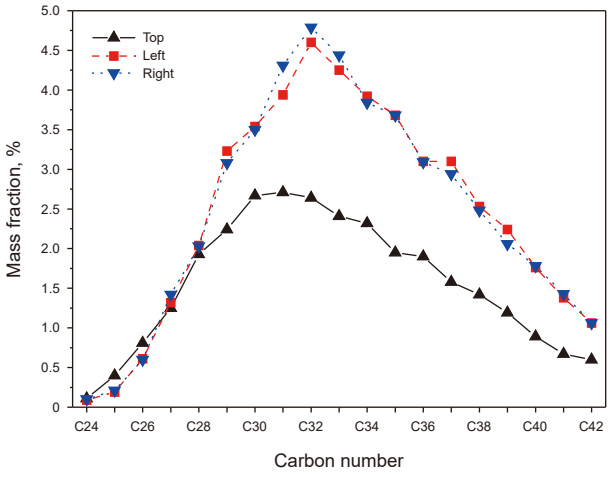

Fig. 15. Carbon number distribution of deposits at different radial positions on the pipe wall.

3.3.1.2. Effect of deposition time. Fig. 16 shows the morphology distribution of the deposit layer on the inner pipe wall cross-section after 4, 12, and 24 h of deposition under superficial oil-phase velocity U_{so} = 0.09 m/s and superficial water-phase velocity U_{sw} = 0.11 m/s. The deposit thickness at the pipe crown increases with deposition time. Conversely, the vertical distance from the pipe crown to the bottom of the deposit layer remains essentially constant throughout the deposition period. This indicates that under the given flow conditions, the deposit layer exerts negligible influence on the oil-phase-wetted perimeter.

The wax content of the deposits at the top and side of the pipe wall and all deposits of the test section of the pipe with deposition times of 4, 12 and 24 h were measured by high temperature gas chromatography and are shown in Fig. 17. It can be seen that the wax content of the deposits at the side of the pipe wall was always higher than that at the top of the pipe wall, and the wax content of all deposits in the test section was higher than that at the top of the pipe wall and lower than that at the side of the pipe wall. The wax content of the deposits at the top of the pipe wall, at the sides and in the whole test section of the pipe increased with the deposition time, the wax content of the deposits at the sides increased with the deposition time less than that of the deposits at the top of the pipe wall and in the whole test section, and the wax content of the deposits in the whole test section increased by a roughly equal amount as that at the top of the pipe wall. Since the thickness of the deposition layer at the top of the tube wall is much higher than at the sides of the tube wall, the wax content of the deposition of the test section as a whole depends mainly on the wax content of the deposition at the top of the tube wall.

Figs. 18 and 19 illustrate the pattern of carbon number distribution of the deposition at the top and side of the pipe wall with the deposition time, respectively. It can be seen from the figures that, with the deposition time, more high carbon number components appear in the wax deposition at the top and side of the pipe wall, indicating that there is an “aging” phenomenon in the deposition layer of the oil-water two-phase stratified flow. Comparing Figs. 18

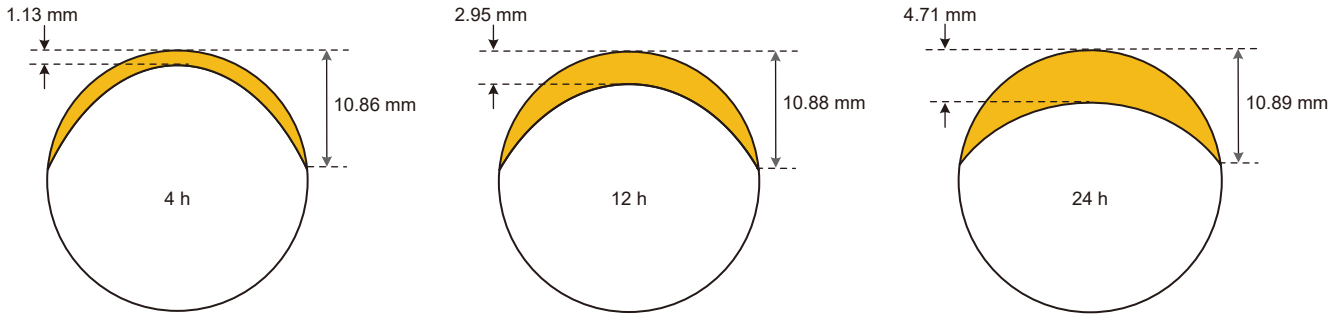

Fig. 16. Morphological distribution of the deposition layer on the inner wall cross-section of the pipeline.

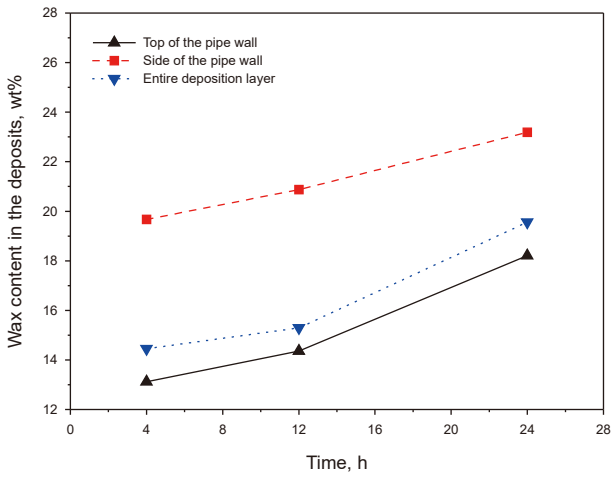

Fig. 17. Diagram of the variation law of wax content in deposition with time on the top and side surfaces of the pipe wall.

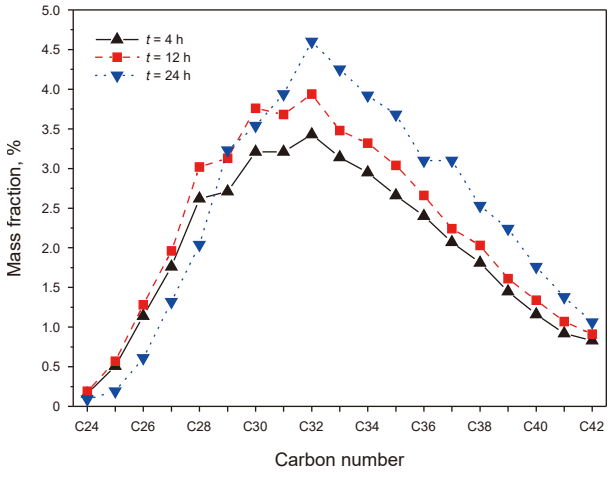

Fig. 19. Carbon number distribution of deposits on the pipe wall side.

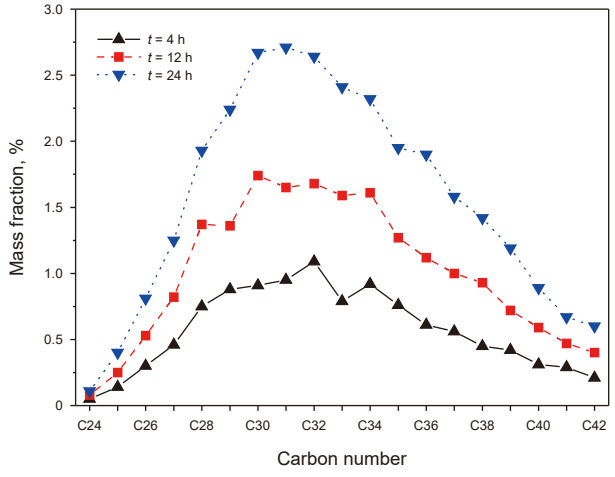

Fig. 18. Carbon number distribution of deposits on the pipe wall top.

and 19, it can be concluded that, compared with the side of the pipe wall, the top of the pipe wall has fewer components in the same deposition time, and the content of high carbon number alkanes is low at the initial moment of deposition, and the "aging" tendency of the deposition layer is more obvious.

3.3.2. *Effect of wate phase superficial velocities on wax deposition*

Wax deposition experiments were conducted at an oil phase superficial velocity U_{so} = 0.15 m/s and wate phase superficial velocities U_{sw} = 0.05, 0.11, and 0.34 m/s, respectively, to investigate the influence of different water phase superficial velocities on wax deposition in stratified oil-water two-phase flow. Fig. 20 presents the variation of deposition mass with deposition time at different water phase superficial velocities for a fixed oil phase superficial velocity of U_{so} = 0.15 m/s. The results show that the deposition mass increases with time. In addition, at the same deposition time, the deposition mass decreases with increasing water phase superficial velocity.

In oil-water two-phase stratified flow, the oil phase occupies only the upper section of the pipe. Consequently, wax deposition occurs exclusively on the pipe wall wetted by the oil phase in this upper region and is absent on the pipe wall wetted by the water phase in the lower section. The area of the pipe wall wetted by the oil phase varies with flow conditions, leading to differences in the surface area covered by wax deposition. Therefore, characterizing the wax deposition rate using the mass of deposits per unit deposition area (i.e., the deposit mass divided by the wetted area where deposition occurs) under stratified oil-water flow conditions provides a more scientifically sound and reasonable approach.

Fig. 21 illustrates the perimeter of the pipe wall wetted by the oil phase in the pipe cross-section under different water phase apparent velocities. The results indicate that this wetted perimeter decreases with increasing water phase superficial velocity but increases with increasing oil phase superficial velocity. This implies that a larger surface area is available for wax deposition as the oil phase superficial velocity increases or the water phase superficial velocity decreases. This observed trend agrees with

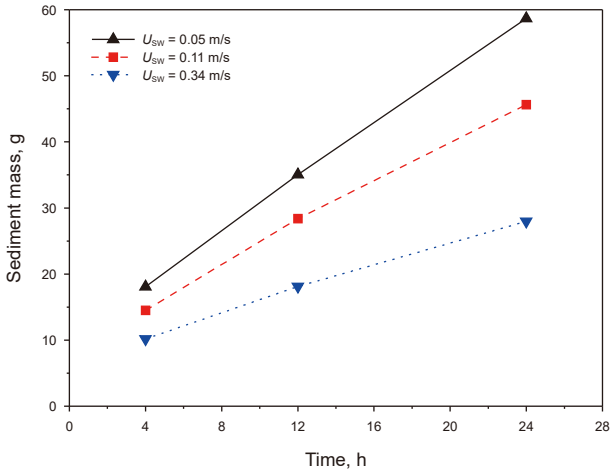

Fig. 20. Diagram of the variation law of wax deposition mass with time under different wate phase superficial velocities.

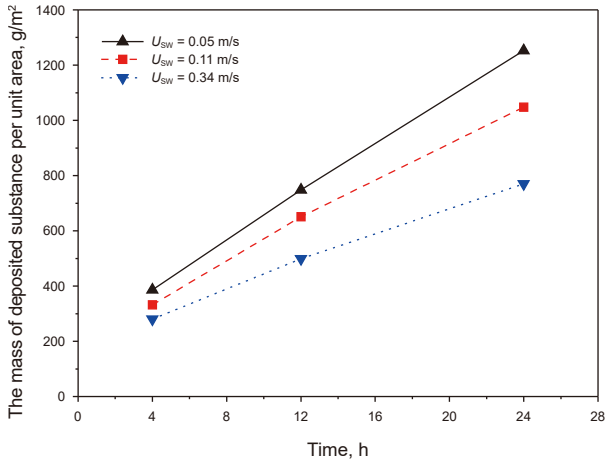

Fig. 22. Diagram of the variation law of wax deposition mass per unit area with time under different wate phase superficial velocities.

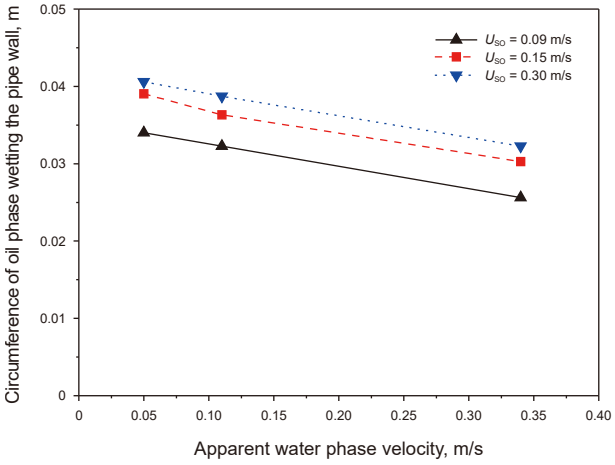

Fig. 21. The perimeter of the pipe wall wetted by the oil phase in the pipe cross-section under different water phase apparent velocities.

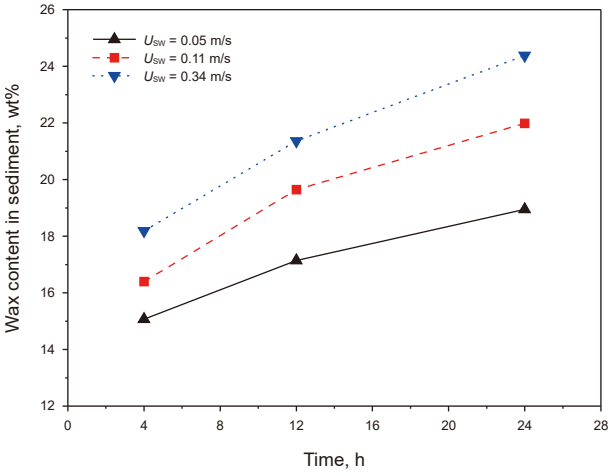

Fig. 23. Diagram of the variation law of wax content in deposition with time under different wate phase superficial velocities.

calculations from the stratified oil-water two-phase flow model developed by Ullmann et al. (2004). Additionally, Santos et al. (2019) and Edomwonyi-Out and Angeli (2015) also experimentally observed that the perimeter wetted by the oil phase decreases with increasing water phase superficial velocity.

Fig. 22 shows the variation of wax deposition mass per unit area with time under different water phase superficial velocities for a fixed oil phase superficial velocity $U_{so} = 0.15$ m/s. As observed for the total deposition mass trend, the deposition mass per unit area decreases with increasing water phase superficial velocity This trend is consistent with the experimental results of Hoffmann et al. (2012) for wax deposition under oil-water two-phase stratified flow. Specifically, Hoffmann et al. (2012) measured deposition mass per unit area values of 1643.8 and 705.2 g/m^2 in oil-water two-phase stratified flow loop experiments at oil phase superficial velocities of 0.33 m/s combined with water phase superficial velocities of 0.33 and 0.98 m/s, respectively.

Fig. 23 presents the wax content in deposition under different water phase superficial velocities. The results demonstrate that the wax content in the deposition layer gradually increases with increasing water phase superficial velocity. At a constant oil phase superficial velocity, the oil volume fraction in the pipe cross-section decreases as the water phase superficial velocity increases. This increase in the actual oil-phase flow velocity leads to higher shear stress on the deposition layer surface. Consequently, this promotes the formation of more interlocked solid-phase wax crystals, resulting in a deposition layer with higher shear yield stress, higher hardness, and higher wax content (Yao et al., 2023; Santos et al., 2021).

The diffusive mass flow of wax molecules from the main body of the oil flow to the surface of the deposition layer, J_{wax}, is a key parameter for wax deposition prediction modeling (Soedarmo et al., 2017) and corresponds to the slope of the deposition mass per unit area versus time plot. Fig. 24 shows the variation of the wax molecular diffusive mass flux J_{wax} with time at different water phase superficial velocities for a fixed oil phase superficial velocity $U_{so} = 0.15$ m/s. The results indicate that J_{wax} decreases with deposition time. This decrease occurs because the deposition layer on the pipe inner wall increases thermal resistance, reducing heat transfer from the oil flow to the environment. Additionally, J_{wax} decreases with increasing water phase superficial velocity, which aligns with the experimental trend observed in Fig. 22.

The influence of different water phase superficial velocities on wax deposition across the pipe cross-section under oil-water two-phase stratified flow was also examined. Fig. 25 presents the

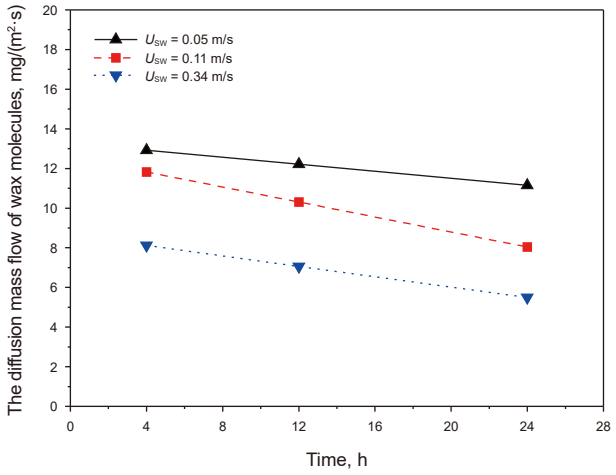

Fig. 24. Diagram of the variation law of diffusive mass flux of wax molecules with time under different wate phase superficial velocities.

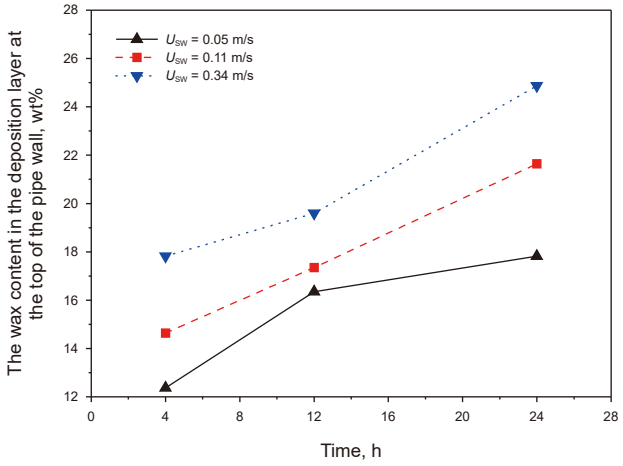

Fig. 26. Diagram of the variation law of wax content in the deposition layer on the top of the pipe wall with time under different wate phase superficial velocities.

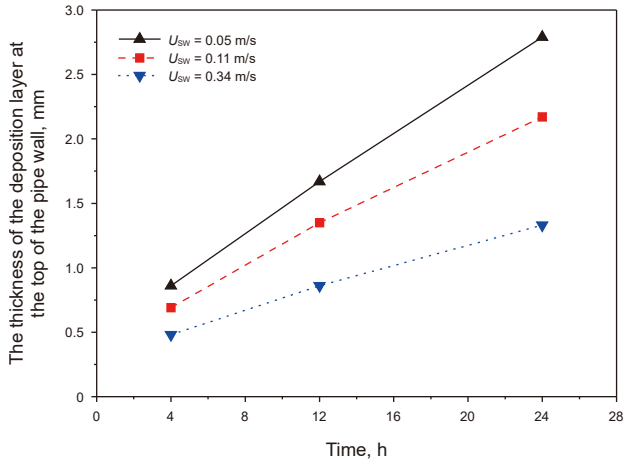

Fig. 25. Diagram of the variation law of the thickness of the deposition layer on the top of the pipe wall with time under different wate phase superficial velocities.

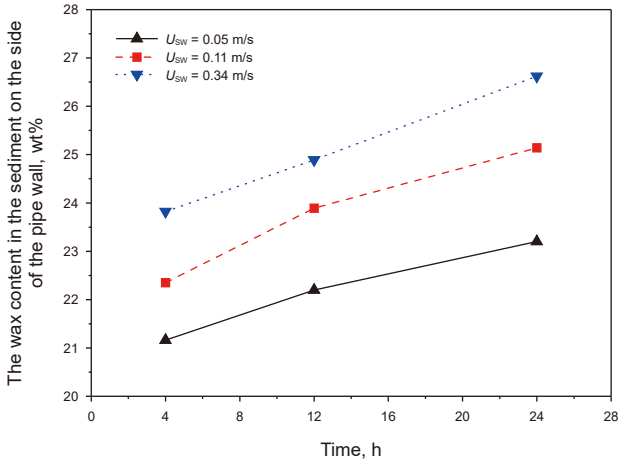

Fig. 27. Diagram of the variation law of wax content in the deposition layer on the side of the pipe wall with time under different wate phase superficial velocities.

variation of deposition layer thickness at the top of the pipe wall with deposition time for an oil phase superficial velocity U_{so} = 0.15 m/s and different water phase superficial velocities. It can be observed that the deposition layer thickness increases with time. Furthermore, at the same deposition time, the deposition layer thickness decreases with increasing water phase superficial velocity.

Figs. 26 and 27 present the variation of wax content in the deposits on the top and side of the pipe wall, respectively, with deposition time for different water phase superficial velocities at a fixed oil phase superficial velocity. It can be observed that the deposits at both the top and side locations exhibit the "aging" phenomenon: the wax content increases with deposition time, consistent with the trend shown in Fig. 17. Furthermore, at the same deposition time, the wax content on both the top and side of the pipe wall increases with increasing water phase superficial velocity.

This increase in wax content is primarily attributed to the following sequence of effects. As the water phase superficial velocity increases, the oil volume fraction in the pipe cross-section decreases, reducing the flow area available for the oil phase. Consequently, the actual oil phase superficial velocity increases. This higher flow velocity generates greater shear stress on the deposition layer surface. The increased shear stress promotes the formation of a deposition layer with higher shear yield stress and higher wax content.

Figs. 28 and 29 present the carbon number distributions of the deposits on the top and side of the pipe wall, respectively. The results show that the content of high-carbon-number components in the deposits increases with increasing water phase superficial velocity. This trend further confirms that an increase in water phase superficial velocity promotes the "aging" phenomenon observed in the deposition layer at both the top and side locations. Furthermore, comparison of the carbon number distributions between the top and side deposits reveals that the water phase superficial velocity has a more pronounced effect on the carbon number distribution at the side of the pipe wall.

3.3.3. *Effect of oil phase superficial velocities on wax deposition*

Wax deposition experiments were conducted at U_{sw} = 0.34 m/s and U_{so} = 0.09, 0.15, and 0.30 m/s, respectively, to investigate the influence of different oil phase superficial velocities on wax deposition under oil-water two-phase stratified flow. Figs. 30 and 31 present the variation of deposition mass and deposition mass per unit area with deposition time for different U_{so} at a fixed

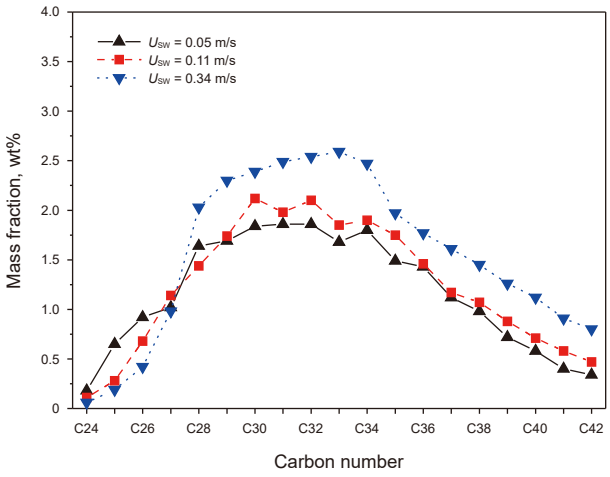

Fig. 28. The distribution of carbon numbers in deposition deposited on the top of the pipe wall under different wate phase superficial velocities.

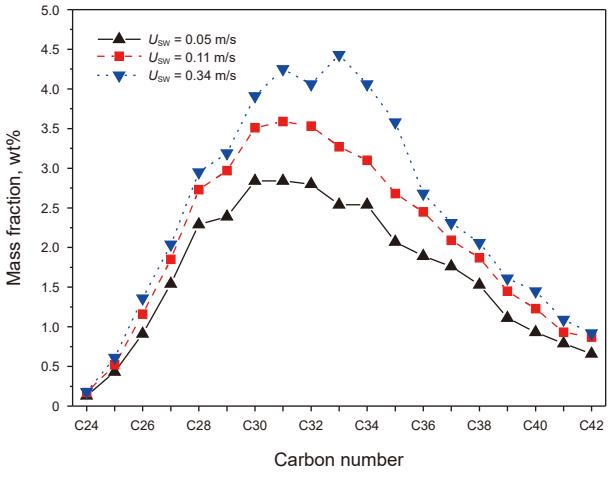

Fig. 29. The distribution of carbon numbers in deposition deposited on the side of the pipe wall under different wate phase superficial velocities.

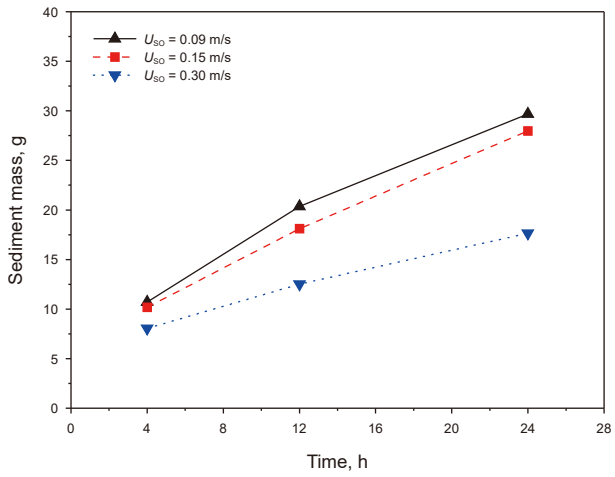

Fig. 30. Diagram of the variation law of wax deposition mass with time under different oil phase superficial velocities.

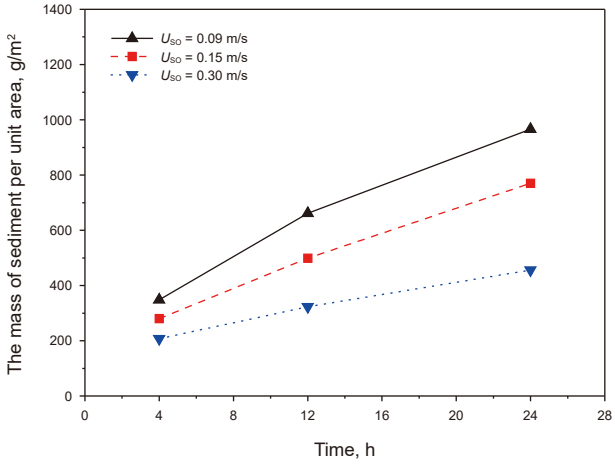

Fig. 31. Diagram of the variation law of wax deposition mass per unit area with time under different oil phase superficial velocities.

U_{sw} = 0.34 m/s. The results show that both deposition mass and deposition mass per unit area increase with time. However, at the same deposition time, deposition mass and deposition mass per unit area decrease with increasing oil phase superficial velocity.

Studies by the research group led by Prof. Fogler at the University of Michigan, USA (Huang et al., 2011a, 2011b, 2011c; Lu et al., 2012; Zheng et al., 2013), demonstrate that the growth rate of the wax deposition layer is primarily governed by the diffusive mass flow of wax molecules, J_{wax}, from the bulk oil flow to the deposition layer surface. Furthermore, these studies indicate that wax mass transfer normalized per unit area of the deposit layer is the direct cause of pipeline wax deposition formation. Therefore, the variation of deposit mass per unit area with time and oil phase superficial velocity is mainly attributable to the variation in J_{wax}. Fig. 32 shows the variation of J_{wax} with time for different U_{so} at a fixed U_{sw} = 0.34 m/s. The results indicate that J_{wax} decreases with increasing U_{so}. This trend is consistent with the experimental observations presented in Fig. 31.

Fig. 33 shows the oil-phase wetted perimeter in the pipe cross-section at different U_{so}. The results indicate that the oil-phase wetted perimeter (S_o) increases with increasing U_{so}. This implies greater surface area availability for wax deposition at higher U_{so}.

Under oil-water two-phase stratified flow conditions, a higher U_{so} provides more surface area for wax deposition. At the same deposition time, the total deposition mass decreases with increasing U_{so}. This phenomenon occurs because the reduction in deposition mass per unit area with increasing U_{so} exceeds the magnitude of the increase in available deposition surface area. Fig. 34 presents the wax content of deposits at different U_{so}. The results demonstrate that the wax content in deposition layer gradually increases with increasing U_{so}. The higher U_{so} generates increased shear stress on the deposition layer surface. Consequently, the resulting deposit exhibits higher shear yield stress, greater hardness, and elevated wax content.

Similarly, the influence of oil-phase apparent flow rate on wax deposition on the pipe cross-section under stratified flow was studied. Fig. 35 presents the variation of deposition layer thickness on the top of the pipe wall with deposition time for different U_{so} at a fixed U_{sw} = 0.34 m/s. The results reveal a similar trend to that observed for water-phase velocity variations: the thickness increases with deposition time but decreases with increasing.

Figs. 36 and 37 respectively exhibit the wax content change rule of the deposition on the top and side of the pipe cross-section with the deposition time under different oil phase apparent flow rates.

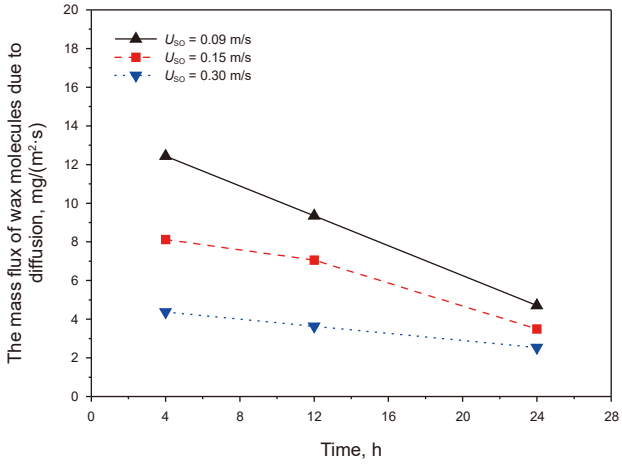

Fig. 32. Diagram of the variation law of the mass flux of wax molecules due to diffusion with time under different oil phase superficial velocities.

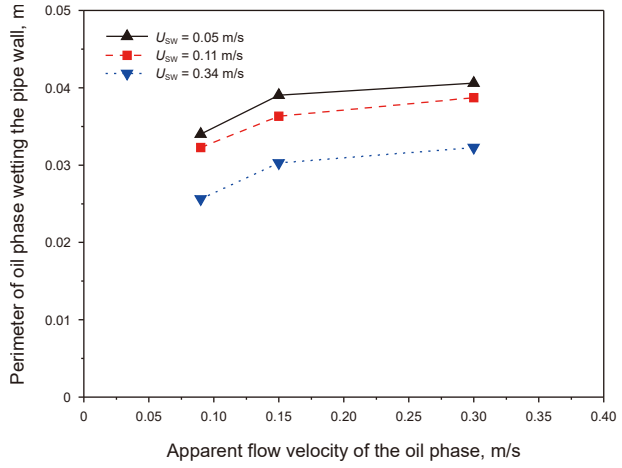

Fig. 33. The perimeter of the pipe wall wetted by the oil phase in the pipe cross-section under different oil phase apparent velocities.

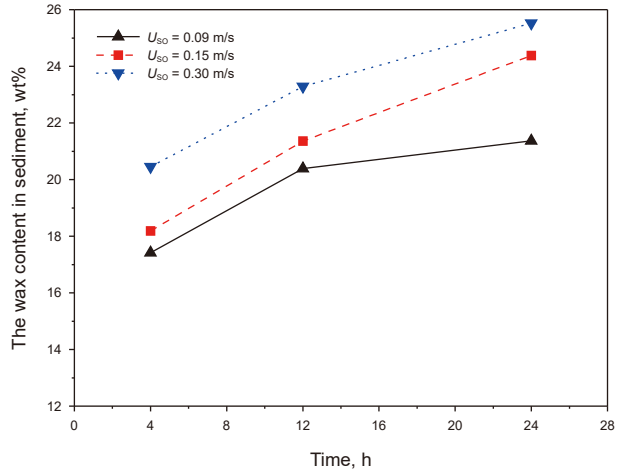

Fig. 34. Diagram of the variation law of wax content in deposition with time under different oil phase superficial velocities.

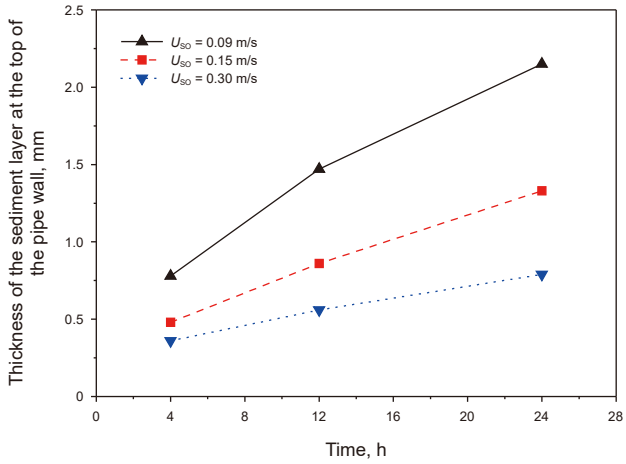

Fig. 35. Diagram of the variation law of the thickness of the deposition layer on the top of the pipe wall and time under different oil phase superficial velocities.

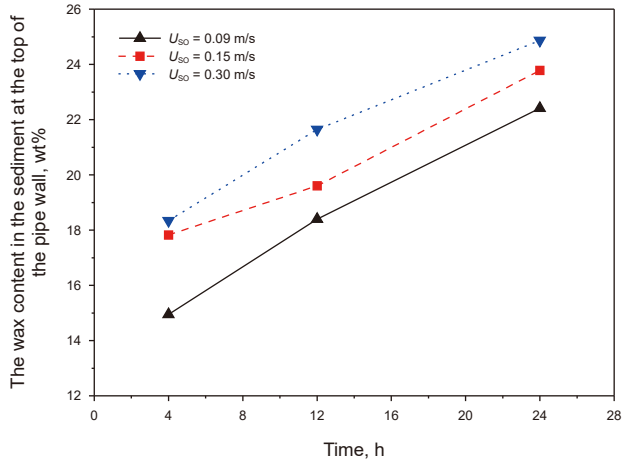

Fig. 36. Diagram of the variation law of wax content in the deposition layer on the top of the pipe wall with time under different oil phase superficial velocities.

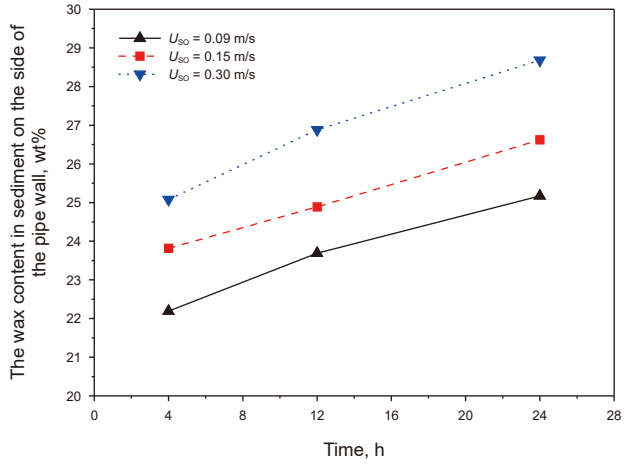

Fig. 37. Diagram of the variation law of wax content in the deposition layer on the side of the pipe wall with time under different oil phase superficial velocities.

It can be seen that the deposits at the top and side of the pipe cross-section wall show the phenomenon of "aging" of the deposited layer. Under the same deposition time, with the increase of the apparent oil phase flow rate, the wax content of the deposits at the top and side of the pipe cross-section also shows an increasing trend. This is mainly due to the higher shear stress on the surface of the deposited layer by the increase of the actual flow rate of the oil phase, which leads to higher shear yield stress in the deposited layer and higher content of wax crystals in the deposits.

Figs. 38 and 39 show the carbon number distribution patterns of the deposition on the top and side of the pipe wall in the pipe cross-section at different apparent oil-phase flow rates, respectively. The content of high carbon number components in the deposition increases with the increase of oil-phase apparent flow rate, which also indicates that the oil-phase apparent flow rate promotes the "aging" of the deposition layer at the top and side of the pipe wall. This is not in agreement with the pattern of liquid-phase apparent flow rate influence on the wax deposition characteristics on the pipe cross-section in oil-gas two-phase stratified flow. In oil-gas two-phase stratified flow, the increase of liquid-phase apparent flow rate has less effect on the carbon number distribution of the bottom and side deposits of the pipe. This is mainly due to the compressibility of the gas phase, and an increase in the apparent liquid-phase flow rate causes only a small increase in the actual liquid-phase flow rate. However, an increase in the apparent flow rate of the oil phase during oil-water two-phase stratified flow causes a larger increase in the actual flow rate of the oil phase, which leads to a larger change in the shear stress of the oil flow on the surface of the deposition layer.

3.4. Comparative analysis of wax deposition in single-phase pipe flow and two-phase pipe flow

In single-phase wax deposition, the oil phase actual velocity is closely related to the shear effect and heat and mass transfer characteristics of the oil flow (Wang et al., 2024; Santos et al., 2021). Under oil-water two-phase stratified flow, both the oil and water phases occupy only a portion of the pipe cross-section, and the superficial velocity cannot characterize the overall flow state of the medium. Therefore, to further investigate the wax deposition behavior in stratified flow and study the differences between single-phase and two-phase wax deposition, it is necessary to analyze the effect of the oil-phase actual velocity on wax

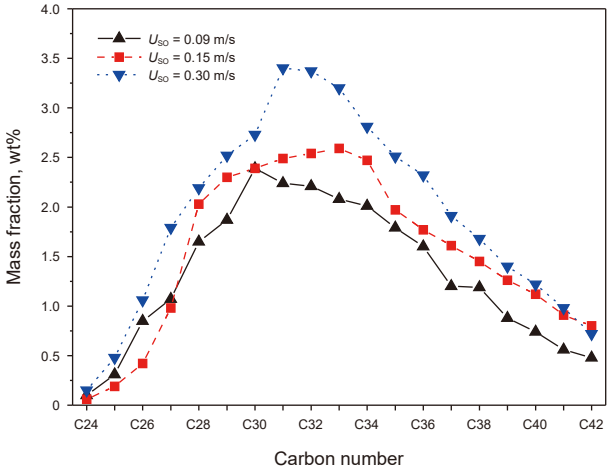

Fig. 38. The distribution of carbon numbers in deposition deposited on the top of the pipe wall under different oil phase superficial velocities.

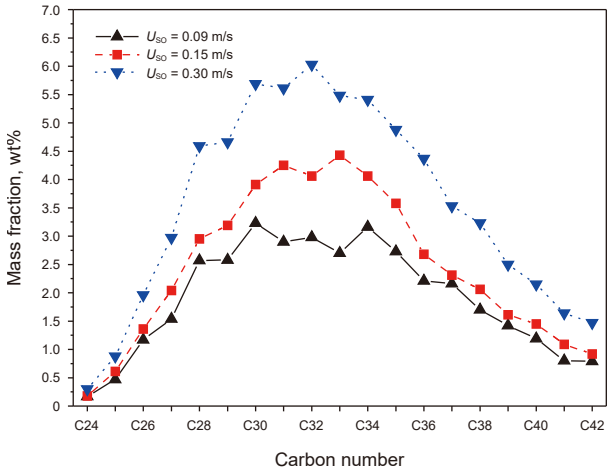

Fig. 39. The distribution of carbon numbers in deposition deposited on the side of the pipe wall under different oil phase superficial velocities.

deposition in oil-water two-phase stratified flow. Under stratified flow conditions, the oil phase actual velocity (U_o) is given by:

$$U_O = \frac{U_{SO}}{H_O} \tag{1}$$

where H_o is the oil content of the pipe cross-section.

Fig. 40 presents the correspondence between the oil phase actual velocity and the water phase superficial velocity during oil-water two-phase stratified flow for the experimental conditions specified in Table 2. It can be seen that oil phase actual velocity increases with the increase of the superficial velocity of the water and oil phases.

Fig. 41 compares the wax deposition mass per unit area after 24 h under single-phase flow and oil-water two-phase stratified flow conditions. The results indicate that for similar oil phase actual velocities, the deposition thickness in oil-water two-phase stratified flow is smaller than that in single-phase flow. This observation aligns with the conclusion of Huang et al. (2011) from their wax deposition model for oil-water stratified flow in parallel plates, namely that the presence of the water phase significantly alters heat and mass transfer characteristics during flow, thereby reducing the wax deposition rate compared to single-phase conditions. In both single-phase and two-phase flow, the mass of deposition per unit

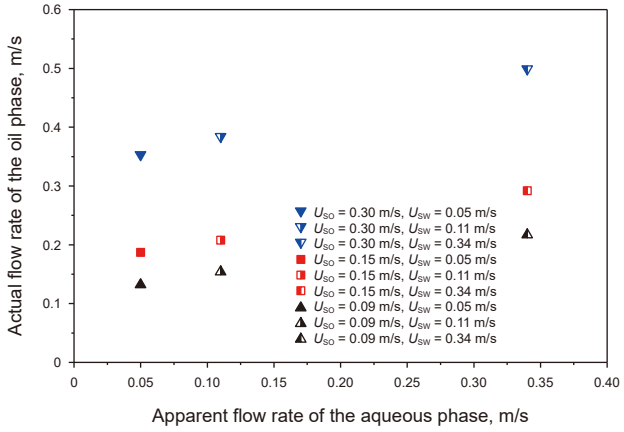

Fig. 40. The correspondence between the oil phase actual velocity and the water phase superficial velocity.

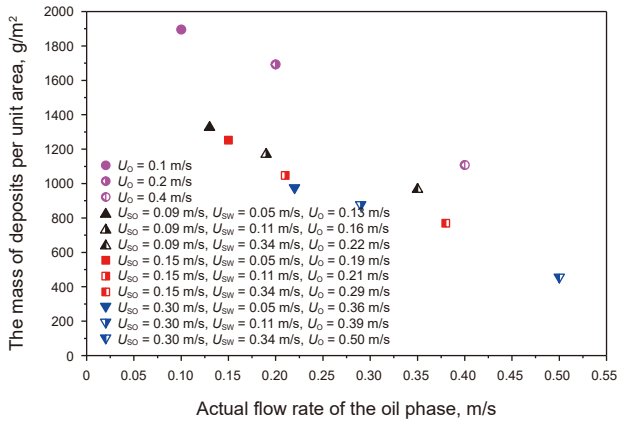

Fig. 41. Wax deposition mass per unit deposition area under single-phase flow and oil-water two-phase stratified flow conditions.

area decreases as the oil phase actual velocity increases. However, the reduction in deposition mass observed in two-phase flow is more pronounced than that in single-phase flow.

Fig. 42 shows the difference in wax content of deposits after 24 h between single-phase flow and oil-water two-phase stratified flow conditions. The results indicate that under single-phase flow, the wax content increases with increasing actual oil-phase flow velocity, exhibiting a relatively gentle growth trend. Similarly, in oil-water two-phase stratified flow, the wax content demonstrates a more pronounced increase with increasing the oil phase actual velocity.

The comparison of wax deposition in oil-water two-phase stratified flow versus single-phase flow indicates that the wax deposition model for two-phase flow, which is based solely on local heat transfer parameters and the physical properties of fluid mixing from the single-phase flow model, exhibits significant discrepancies. Therefore, it is essential to accurately characterize the influences of flow dynamics, as well as heat and mass transfer properties, on wax deposition during oil-water two-phase stratified flow in order to reliably predict wax accumulation in pipelines operating under two-phase conditions.

4. Conclusions

This study experimentally investigated the wax deposition behavior under oil-water laminar stratified flow conditions. The key findings and their practical implications are summarized as follows:

(1) The wax deposition layer exhibits a distinct crescent-shaped profile, forming exclusively on the upper oil-contact pipe wall, with no deposition on the water-wetted bottom section. This non-uniform distribution implies that pigging operations and tools can be strategically optimized to focus on the upper pipeline section, potentially enhancing cleaning efficiency and reducing operational costs.

(2) The superficial velocities of both oil and water phases exhibit a dual effect: they suppress the wax deposition rate, reducing the layer thickness and mass, yet enhance the wax content and heavy component concentration in the deposits. Notably, the water phase velocity plays a more critical role in determining the composition of sidewall deposits compared to the oil phase.

(3) Compared to single-phase flow, oil-water two-phase flow yields a significantly thinner deposition layer due to altered heat and mass transfer. Although the deposit mass per unit area decreases with increasing oil-phase actual velocity in both regimes, this suppressing effect is markedly more pronounced under two-phase flow conditions. This finding highlights the necessity of developing or calibrating predictive models specifically for stratified flow conditions, as relying on single-phase models may lead to significant overprediction of deposition risks in oil-water pipelines.

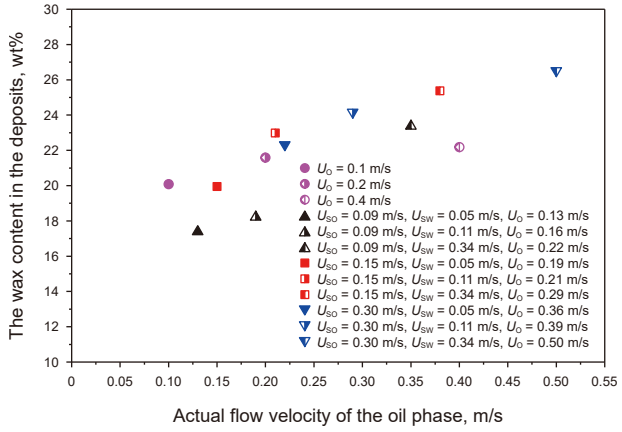

Fig. 42. The wax content in the deposition under single-phase flow and oil-water two-phase stratified flow conditions.

CRediT authorship contribution statement

Hui-Shu Liu: Writing – original draft, Validation, Funding acquisition, Conceptualization. **Ji-Miao Duan:** Writing – original draft, Resources, Funding acquisition. **Yong-Xiang Huang:** Supervision, Investigation. **Hao-Nan Li:** Writing – review & editing, Writing – original draft, Investigation. **Hui-Rong Huang:** Validation, Software. **Shi-Ming Chen:** Supervision, Methodology. **Jun-Zhe Jiang:** Methodology, Data curation.

Declaration of competing interests

The authors declare that they have no known competing financial interests or personal relationships that could have appeared to influence the work reported in this paper.

Acknowledgement

This research was funded by the Natural Science Foundation of China (52272338, 52302422 and 52302402), the Natural Science Foundation of Chongqing, China (CSTB2024NSCQ-QCXMX0080 and CSTB2024NSCQ-MSX1039), the Science and Technology Research Program of Chongqing Municipal Education Commission (KJZD-M202501502), and the Research Foundation of Chongqing University of Science and Technology (ckrc20241204).

Appendix A. Supplementary data

Supplementary data to this article can be found online at https://doi.org/10.1016/j.petsci.2026.01.016.

References

Akbari, A., Kazemzadeh, Y., Martyushev, D.A., Cortes, F., 2024. Using ultrasonic and microwave to prevent and reduce wax deposition in oil production. Petrol 10 (4), 584–593. https://doi.org/10.1016/j.petlm.2024.09.002.

Anosike, C.F., 2007. Effect of Flow Patterns on oil-water Flow Paraffin Deposition in Horizontal Pipes. University of Tulsa.
Bordalo, S.N., Oliveira, R.D., 2007. Experimental Study of oil/water Flow with Paraffin Precipitation in Submarine Pipelines. In: SPE Annual Technical Conference and Exhibition, SPE-110810-MS. https://doi.org/10.2118/110810-MS.
Chi, Y., Sarica, C., Daraboina, N., 2019. Experimental investigation of two-phase gas-oil stratified flow wax deposition in pipeline. Fuel 247, 113–125. https://doi.org/10.1016/j.fuel.2019.03.032.
Duan, J., Liu, H., Jiang, J., Liu, H., Jiang, J., Xue, S., Wu, J., Gong, J., 2017. Numerical prediction of wax deposition in oil–gas stratified pipe flow. Int. J. Heat Mass Tran. 105, 279–289. https://doi.org/10.1016/j.ijheatmasstransfer.2016.09.082.
Edomwonyi-Out, L.C., Angeli, P., 2015. Pressure drop and holdup predictions in horizontal oil–water flows for curved and wavy interfaces. Chem. Eng. Res. Des. 93, 55–65. https://doi.org/10.1016/j.cherd.2014.06.009.
Goncalves, G.F.N., Matar, O.K., 2022. Mechanistic modelling of two-phase slug flows with deposition. Chem. Eng. Sci. 259 (0), 117796. https://doi.org/10.1016/j.ces.2022.117796.
Hoffmann, R., Amundsen, L., Huang, Z., et al., 2012. Wax deposition in stratified oil/water flow. Energy Fuels 26 (6), 3416–3423. https://doi.org/10.1021/ef2018989.
Huang, Z., Lee, H.S., Senra, M., 2011a. A fundamental model of wax deposition in subsea oil pipelines. AIChE J. 57 (11), 2955–2964. https://doi.org/10.1002/aic.12517.
Huang, Z., Lu, Y., Hoffmann, R., et al., 2011b. The effect of operating temperatures on wax deposition. Energy Fuels 25 (11), 5180–5188. https://doi.org/10.1021/ef201048w.
Huang, Z., Senra, M., Kapoor, R., et al., 2011c. Wax deposition modeling of oil/water stratified channel flow. AIChE J. 57 (4), 841–851. https://doi.org/10.1002/aic.12307.
Lekomtsev, A.V., Ilyushin, P.Y., Martyushev, D.A., 2018. Experience of implementing an intensifying device on the developed Mobile well production treatment unit. Chem. Petrol. Eng. 54 (3–4), 213–219. https://doi.org/10.1007/s10556-018-0465-4.
Li, R., Huang, Q., Zhang, D., Zhu, X., Shan, J., Wang, J., 2020. An aging theory-based mathematic model for estimating the wax content of wax deposits using the Fick's second law. AIChE J. 66 (4), 16892. https://doi.org/10.1002/aic.16892.
Lu, Y., Huang, Z., Hoffmann, R., et al., 2012. Counterintuitive effects of the oil flow rate on wax deposition. Energy Fuels 26 (7), 4091–4097. https://doi.org/10.1021/ef3002789.
Piroozian, A., Hemmati, M., Ismail, I., Manan, M.A., Rashidi, M.M., Mohsin, R., 2017. An experimental study of flow patterns pertinent to waxy crude oil-water two-phase flows. Chem. Eng. Sci. 164 (1), 313–332. https://doi.org/10.1016/j.ces.2017.02.026.
Quan, Q., Wang, W., Wang, P., Duan, J., Yang, J., Yao, H., Gong, J., 2015. Wax deposition from emulsion-water in stratified flow. Petrol. Sci. Technol. 33 (6), 749–755. https://doi.org/10.1080/10916466.2015.1007381.
Santos, D.S., Faia, P.M., Garcia, F.A.P., Rasteiro, M.G., 2019. Oil/water stratified flow in a horizontal pipe: simulated and experimental studies using EIT. J. Petrol. Sci. Eng. 174 (0), 1179–1193. https://doi.org/10.1016/j.petrol.2018.12.002.
Santos, G., Daraboina, N., Sarica, C., 2021. Dynamic microscopic study of wax deposition: particulate deposition. Energy Fuels 35 (15), 12065–12074. https://doi.org/10.1021/acs.energyfuels.1c01684.
Shafiei, M., Kazemzadeh, Y., Martyushev, D.A., Dai, Z., Riazi, M., 2023. Effect of chemicals on the phase and viscosity behavior of water in oil emulsions. Sci. Rep. 13 (1), 2045–2322. https://doi.org/10.1038/s41598-023-31379-0.
Soedarmo, A.A., Daraboina, N., Sarica, C., 2017. Validation of wax deposition models with recent laboratory scale flow loop experimental data. J. Petrol. Sci. Eng. 149, 351–366. https://doi.org/10.1016/j.petrol.2016.10.017.
Ullmann, A., Goldstein, A., Zamir, M., Brauner, N., 2004. Closure relations for the shear stresses in two-fluid models for laminar stratified flow. Int. J. Multiphas. Flow 30 (7–8), 877–900. https://doi.org/10.1016/j.ijmultiphaseflow.2004.03.008.
Wang, J., Hao, Y., Zhu, B., Han, T., Li, Z., Zhang, J., 2022. Crystalline behavior of paraffin wax. J. Phys. Chem. B 126 (4), 985–995. https://doi.org/10.1021/acs.jpcb.1c10000.
Wang, C., Ma, Q., Lv, X., Zhang, J., Liu, Y., Zhou, S., 2024. Experimental study on wax deposition of highly paraffinic oil in intermittent gas-oil flow in pipelines. Pet. Sci. 21 (3), 2080–2088. https://doi.org/10.1016/j.petsci.2024.01.003.
Yao, B., Zhu, H., Yan, B., Li, C., Yang, F., Sun, G., Zeng, H., 2023. Pre-heating temperature induced flowability and wax deposition characteristics of crude oil adding wax inhibitors. Pet. Sci. 4, 2468–2478. https://doi.org/10.1016/j.petsci.2023.02.030.
Zheng, S., 2017. Wax Deposition from Single-phase Oil Flows and water-oil Two-phase Flows in Oil Transportation Pipelines. University of Michigan. https://hdl.handle.net/2027.42/137101.
Zheng, S., Zhang, F., Huang, Z., et al., 2013. Effects of operating conditions on wax deposit carbon number distribution: theory and experiment. Energy Fuels 27 (12), 7379–7388. https://doi.org/10.1021/ef402051n.